Multilayer structure of nitrogen adsorbed on graphite

S.- K. Wang, J. C. Newton, R. Wang,* H. Taub, and J. R. Dennison†
Department of Physics and Astronomy, University of Missouri–Columbia, Columbia, Missouri 65211

H. Shechter
Physics Department and Solid State Institute, Technion–Israel Institute of Technology, Haifa 32000, Israel
(Received 19 September 1988)

Elastic neutron diffraction has been used to study the structure and layering of nitrogen films adsorbed on the (002) surfaces of an exfoliated graphite substrate. The neutron-diffraction pattern of the fully compressed monolayer at a coverage $\Theta=1.67$ layers and a temperature $\lesssim 11$ K which we reported earlier has been reanalyzed (unity coverage corresponds to a complete layer having the commensurate $\sqrt{3}\times\sqrt{3}$ structure). We now find it to be consistent with a four-sublattice pinwheel structure as well as the two-sublattice herringbone structure which we found previously. Below 11 K, we infer crystallization of the bilayer at Θ between 2.6 and 3.3 layers. As the coverage is increased further, diffraction peaks from bulk particles are first observed at $\Theta\simeq 3.7$ layers, and their intensity increases linearly with Θ up to 10 layers. It is suggested that two amorphous or highly disordered layers of N_2 may adsorb above the fully compressed monolayer prior to bilayer crystallization and a single such layer may adsorb above the bilayer prior to bulk nucleation. From analysis of the diffraction pattern at $\Theta=3.3$ layers, we infer that the bilayer crystal, like the fully compressed monolayer, is slightly distorted from hexagonal symmetry. The two N_2 layers are commensurate with each other and have the same density, which is slightly less than that of the fully compressed monolayer. While we are unable to reach a definitive conclusion on the type of orientational ordering in the bilayer, we present some arguments favoring a pinwheel structure, possibly with more orientational disorder in the first layer than in the second. At coverages $\Theta=6.4$ and 8.0 layers, we find no change in the bulk peak intensities at 23.4 K, where a large heat-capacity peak has been observed. We conclude that a layering transition does not occur at this temperature and suggest instead that the heat-capacity peak may result from the melting of the second layer. Based on this interpretation, we propose a new phase diagram for the N_2-graphite system which is consistent with both heat-capacity and neutron-diffraction data.

I. INTRODUCTION

Nitrogen (N_2) adsorbed on the basal plane surfaces of graphite provides one of the most attractive systems for theoretical investigations of molecular orientational ordering in physisorbed films. Accurate models of the intermolecular and molecule-substrate interactions for this simple diatomic molecule have allowed detailed computer simulations of the monolayer and bilayer structures as reviewed in Ref. 1. On the other hand, experimental confirmation of the theoretically predicted molecular orientations in the various monolayer phases of N_2 on graphite has been more difficult to obtain. As we have discussed previously,[1] both low-energy electron diffraction (LEED) and x-ray diffraction have serious shortcomings for determining the orientation of the adsorbed N_2 molecule. LEED suffers from multiple-scattering effects which complicate the interpretation of the diffracted beam intensities. Since both electrons and x rays scatter from the electron charge cloud, the diffraction patterns are attenuated at large wave vectors by the molecular form factor.

Elastic neutron diffraction has some advantages over both LEED and x-ray scattering for investigating molecular orientational ordering in monolayers of nearly spherical molecules.[1] Because neutrons scatter from pointlike nuclei rather than the electron charge cloud of the molecule, the neutron-diffraction patterns are not attenuated by the molecular form factor. Nuclear scattering also results in greater sensitivity of the higher-order Bragg reflections to the molecular orientation. The molecule appears as a dumbbell to neutrons rather than having the nearly spherical shape of the electron charge cloud. Thus some of the higher-order Bragg reflections which are undetectable in LEED and x-ray experiments can be quite sensitive to the molecular orientation.

In our previous experiments,[1] we were able to infer the molecular orientations at low temperature in the commensurate (C) and uniaxial incommensurate (UI) monolayer phases of N_2 in which the molecules lie with their N—N bond parallel to the graphite (002) surface in a two-sublattice herringbone (HB) arrangement. The in-plane azimuthal orientation of the molecule could be determined with an accuracy of about $\pm 5°$. With somewhat less certainty, we also determined the molecular orientations in the fully compressed monolayer or triangular incommensurate (TI) phase. In this case, we found a "two-out" HB structure in which both molecules in the unit cell have their N—N bond tilted with respect to the surface.

This paper describes neutron-diffraction experiments extending our study of the structure of N_2 films adsorbed on graphite at low temperature to coverages above that of the fully compressed monolayer. It addresses the questions of how thick a N_2 film can grow on the graphite basal plane surface and what is its multilayer structure. To our knowledge, the bilayer or, in fact, any multilayer structure of an orientationally ordered molecular film has never been determined.

Previous electron-diffraction experiments[2] indicate that N_2 incompletely wets graphite at low temperature. That is, bulk clusters of N_2 are observed to form after the adsorption of two layers on the graphite (002) surface. Although the structure of the N_2 bilayer has not previously been determined experimentally, LEED patterns of the bilayer at a temperature of 15 K do *not* show the systematic absences of spots characteristic of the glide line symmetry in the C monolayer phase.[3] For the HB arrangement of molecules in Fig. 1(a), the glide-line symmetry implies that $\phi_1=\phi_2$ and also that their N—N bond is parallel to the surface [($\beta=0$ in Fig. 1(b)]. Based on their LEED results and the mean-field calculations of Harris and Berlinsky,[4] Diehl and Fain[3] suggested a four-sublattice pinwheel structure for the second layer and a poorly ordered, out-of-plane [$\beta\neq 0$ in Fig. 1(b)] herringbone structure for the first layer.

There have been several computer simulations of the N_2 bilayer structure on graphite. O'Shea and Klein[5] used Monte Carlo calculations to investigate the bilayer structure of point quadrupoles. Two basic models were explored: (1) a "free" bilayer in which the molecular orientations are not subject to a substrate crystal field, and (2) an "in-plane" bilayer in which the substrate crystal field is so strong that the linear quadrupoles of the first layer are constrained to be planar. The ground state of the free bilayer has the same symmetry as two (111) planes of bulk α-N_2. Each layer has the four-sublattice pinwheel configuration illustrated in Fig. 1(c). In the ground state of the in-plane bilayer, the upper layer was found to have an out-of-plane herringbone structure. A pinwheel structure for the second layer has a slightly higher energy.

More realistic potentials were used by Vernov and Steele[6] in their molecular-dynamics simulations of commensurate and uniaxially compressed N_2 bilayers at temperatures of 25 and 35 K. The intermolecular interaction included both a N-N Lennard-Jones potential and an electrostatic quadrupole energy represented by a three point-charge model. The film-substrate interaction was derived by summing a pairwise-atomic potential between a N atom in the bilayer and a graphite C atom. It was expanded as a Fourier series in the graphite basal-plane reciprocal-lattice vectors. Vernov and Steele found a tendency for an in-plane orientation of the molecules in both layers. The effect of the second layer was to flatten the molecules below, eliminating any which might be standing on end. For their model of the potentials and the temperatures of their simulations (≥ 25 K), the commensurate bilayer did not orientationally order with herringbone packing, while the uniaxially compressed films did.

The most recent simulations of the multilayer structure of N_2 on graphite are the Monte Carlo calculations of Kuchta and Etters.[7] For the intermolecular interaction, they use a N-N pair potential of their own construction and a four point-charge model for the quadrupole-quadrupole interaction. Their film-substrate interaction is also more elaborate than that of Vernov and Steele. In addition to the van der Waals contribution between the substrate carbon atoms and the atoms of the adsorbed N_2 molecules, a substrate-mediated N_2-N_2 interaction is included which depends on the dielectric function of the substrate and the dynamic polarizability of the N_2 molecules. Finally, there is a relatively small electrostatic interaction between the N_2 electric multipoles and their images induced in the substrate.

The interaction model of Kuchta and Etters is sufficiently accurate to predict the commensurate (C) in-plane herringbone structure at monolayer coverages. The azimuthal angle ϕ_2 in Fig. 1(a) is calculated to be 134° in the middle of the range determined experimentally.[1] Their principal disagreement with experiment is the failure to predict the fully compressed monolayer structure or nearly triangular incommensurate (TI) phase observed both in the LEED (Ref. 3) and neutron-diffraction[1] experiments. As the areal density ρ is increased above that for the C phase ($\rho=1$), a uniaxial incommensurate (UI) phase is found up to $\rho\simeq 1.06$, in agreement with experiment.[1,3] However, at this density, the monolayer is in coexistence with the bilayer, and the TI phase is never realized. The bilayer structure is com-

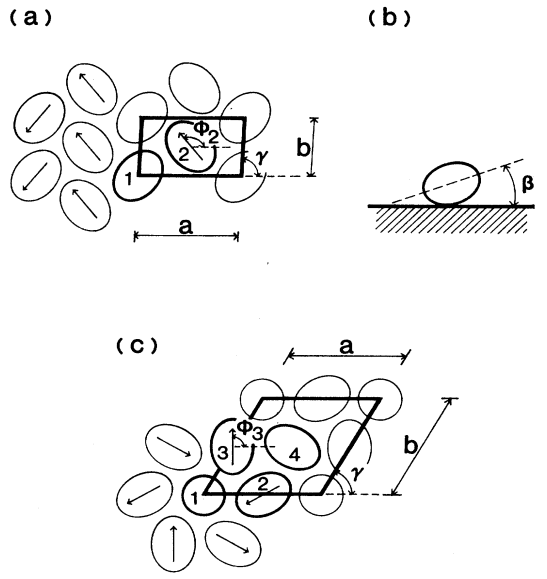

FIG. 1. Projection of a monolayer N_2 unit cell on the graphite surface for (a) the two-sublattice herringbone and (c) the four-sublattice pinwheel models. For each molecule, the azimuthal angle is positive if measured counterclockwise from the positive **a** direction as shown for molecule no. 2 in (a). Note that this definition differs from that in Ref. 1. The head of the arrow on each molecule denotes the end highest above the surface. In (c), molecule no. 1 is perpendicular to the surface. (b) Side view showing tilt of the molecular axis.

plete at $\rho=2.2$, having a distorted herringbone structure [Figs. 1(a) and 1(b)] for the bottom layer and a pinwheel structure [Fig. 1(c)] for the top layer. At low temperature, bulk formation is predicted to occur at densities above bilayer completion.

Although diffraction studies of N_2 multilayers on graphite have been limited, Zhang *et al.*[8] have conducted extensive heat-capacity experiments on multilayer films. These authors also found evidence of incomplete wetting but with a maximum of three film layers before bulk nucleation rather than the two layers inferred in previous diffraction experiments.[2,3] They observed a large and sharp heat-capacity peak at 23.4 K for coverages above two layers and interpreted it as due to a layering transition from a two-layer–plus–bulk to a three-layer–plus–bulk system. They also identified a different temperature for the molecular orientational-disordering transition[3] in the bilayer than in the trilayer phase.

A principal motivation for our work here was to determine the structure of the solid N_2 bilayer and to see whether it might reveal the mechanism inhibiting trilayer growth at low temperature. We also wanted to search for evidence in the neutron-diffraction patterns for a layering transition at 23.4 K as suggested by the heat-capacity experiments.

Our study is organized as follows. In Sec. II we briefly describe the neutron-diffraction technique and data-analysis procedure. In Sec. III, we present the observed diffraction patterns and structural parameters inferred for various models of the fully compressed monolayer and bilayer phases. Our results and conclusions are summarized in Sec. IV with the aid of a phase diagram.

II. EXPERIMENTAL DESCRIPTION

The experimental methods were the same as used in our earlier work.[1] The neutron-diffraction patterns were obtained on the two-axis spectrometer equipped with a position-sensitive detector located at port "*D*" of the University of Missouri Research Reactor. As before, the sample consisted of 40 disks of an exfoliated graphite (Papyex[9]) having a mass of 51 g enclosed in an aluminum cell and mounted in a closed-cycle refrigerator. The Papyex specific surface area was measured to be 21 m^2/g from a vapor-pressure isotherm measurement with N_2 at 78 K. Completion of the *C* monolayer phase was taken to be at the foot of the substep in the isotherm occurring at a pressure of 6.2 Torr as in Ref. 1.

For convenience, we introduce a unit of coverage Θ in addition to the areal density ρ defined above. The coverage $\Theta=1$ corresponds to the number of molecules in a complete layer of the *C* phase in which there is one molecule for every three carbon hexagons (a $\sqrt{3}\times\sqrt{3}$ superlattice) on the graphite basal-plane surface. This is the same unit of coverage used in the heat-capacity studies on N_2 multilayers.[8]

Precautions were taken in loading the sample cell at multilayer coverages to ensure that all the measured gas was adsorbed onto the graphite substrate rather than at a cold point in the capillary to the cell and that the film was well annealed. Typically, the cell was warmed to 100 K and the gas introduced into the capillary, which was heated above this temperature. If necessary, the cell temperature was lowered subsequently in order to expedite filling. But in no case was the cell temperature below 63 K when filling was completed. Finally, the sample was cooled slowly (~ 1 K/min) to the temperature of the diffraction measurement $\lesssim 11$ K.

The profile-analysis technique which we used to fit a model structure factor to the diffraction patterns has been described elsewhere.[1,10–12] Motion of the nuclei about their equilibrium position is assumed to be small enough that it can be treated by a Debye-Waller factor of the form $\exp(-Q^2\langle u^2\rangle)$ where, for simplicity, the mean-square displacement $\langle u^2\rangle$ is taken to be the same for all nuclei.

III. RESULTS

A. Fully compressed monolayer phase

At the outset of our study, it seemed plausible to us that, at low temperature, the structure of the fully compressed monolayer or triangular incommensurate (TI) phase would closely resemble that of the first layer of the N_2 bilayer. From our previous investigations,[1] we had inferred an out-of-plane or "two-out" herringbone structure for the TI phase. Nevertheless, it was difficult to exclude the possibility of a pinwheel structure [Fig. 1(c)] due to the large parameter space which needed to be surveyed (particularly the angles ϕ and β). Thus when recent ground-state calculations[13] favored a pinwheel structure for the fully compressed monolayer and, moreover, gave an explicit parameter set as a starting point for our fitting procedure, we were strongly motivated to reanalyze the neutron-diffraction pattern of the TI phase.

In Fig. 2 the neutron-diffraction pattern of the TI phase ($\Theta=1.67$) at a temperature of 10.5 K is reproduced from Fig. 7 in Ref. 1. The solid curve in Fig. 2(a) is the fit previously obtained[1] to a "two-out" herringbone structure, while that in Fig. 2(b) is the best fit which our reanalysis gave to a pinwheel structure. The lattice and orientational parameters of each model are listed in Table I. Both models yield a density which is about 10% greater than that of the *C* monolayer phase and have a slightly oblique cell [$\gamma\neq 90°$ in Fig. 1(a), $a\neq b$ in Fig. 1(c)]. Thus in each case, a coverage $\Theta=1.67$ would correspond to about 30% of the molecules in the second layer (a coverage $\Theta=1.11$ would occupy the first layer). We estimate the determination of the angles ϕ and β to be about $\pm 8°$. In the case of the pinwheel model, the orientation of molecule no. 1 in the unit cell [Fig. 1(c)] was fixed perpendicular to the surface. For the other three molecules both ϕ and β were allowed to vary starting from their values in the first layer of Bruch's[13] bilayer pinwheel model. The β value was constrained to be the same for these three molecules and was found to be about 10° less than for the herringbone structure. The fits to both the herringbone and pinwheel models in Fig. 2 assume the same Debye-Waller factor of $\langle u^2\rangle=0.03$ Å^2.

Comparing Figs. 2(a) and 2(b) we see that the diffraction profiles calculated for the "two-out" and pinwheel models of the TI phase are quite similar. This

situation contrasts with that found for the in-plane herringbone model of the C phase where the diffraction profiles were sensitive to the azimuthal orientation ϕ of the molecules (cf. Fig. 3 of Ref. 1). We can understand this result qualitatively by recalling that the neutron scatters from the point nuclei of the molecules and that it is the projection of the nuclear positions onto the surface which largely determines the integrated peak intensities. In models of the TI phase where some of the molecules are tilted away from the surface ($\beta \neq 0$), the length of the projection of the N—N bond onto the surface decreases, and hence the sensitivity of the structure factor to the azimuthal angle ϕ is diminished.

In the available scattering windows away from the graphite Bragg peaks, the only differences between the diffraction profiles of the two models appear to be the presence in the pinwheel model of a weak {30} peak calculated at $Q=2.8$ Å^{-1} and also slightly more intensity for a group of unresolved reflections near $Q=7.1$ Å^{-1}. Neither of these features is excluded by the data. Therefore, we conclude that the pinwheel model provides at least as good a fit to the TI phase diffraction pattern as the "two-out" herringbone structure.

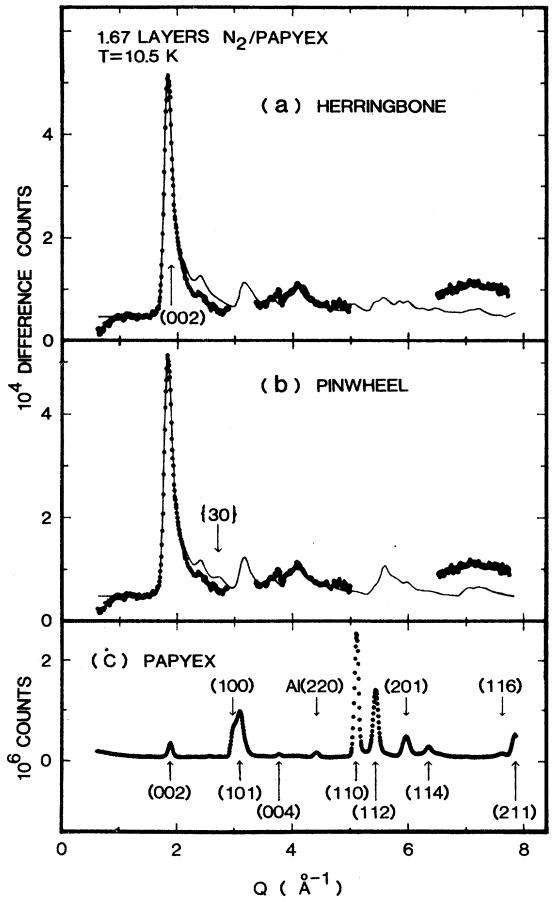

FIG. 2. Neutron-diffraction pattern of 1.67 layers of N_2 on Papyex at 10.5 K after subtraction of the substrate scattering (data same as in Fig. 7 of Ref. 1). The solid curves have been calculated using the parameters listed in Table I for (a) the herringbone model of Ref. 1 and (b) the pinwheel model. A different constant value has been added to the calculated curves above the graphite (002) reflection ($Q=1.88$ Å^{-1}) than below. (c) Diffraction pattern of the bare Papyex. In addition to the graphite peaks, the aluminum (220) peak from the sample cell can be seen. Gaps appear in the film pattern in (a) and (b) in Q ranges of the graphite peaks due to imperfect background subtraction.

TABLE I. Structural parameters for the fully compressed monolayer (TI) phase on graphite inferred from the diffraction pattern at a coverage $\Theta=1.67$ layers and a temperature of 10.5 K (Fig. 2). Both herringbone and pinwheel models are considered. The angles ϕ, β, and γ and lattice constants a and b are defined in Fig. 1. All angles are in degrees. Subscripts denote the molecule number defined in Fig. 1. For the pinwheel structure, z_1 is the height of the center of mass of molecule no. 1 above the plane containing the centers of mass of molecules no. 2, no. 3, and no. 4. L is the "coherence length" defined in Ref. 10 and $\langle u^2 \rangle$ is the mean-square deviation from an equilibrium position appearing in the Debye-Waller factor. The density ρ is dimensionless and is the ratio of the layer areal density to that of the C phase (15.72 Å^2/molecule).

	Herringbone	Pinwheel
a (Å)	7.00	7.94
b (Å)	4.04	8.18
γ	88.5	60.0
ρ	1.112	1.118
ϕ_1	−135	
ϕ_2	135	−150
ϕ_3		90
ϕ_4		−30
β_1	20	90
β_2	20	10
β_3		10
β_4		10
z_1 (Å)		0.294
L (Å)	60	60
$\langle u^2 \rangle$ (Å^2)	0.03	0.03

B. Coverage dependence of the diffraction patterns above monolayer completion

Neutron-diffraction patterns at coverages $\Theta=1.67$, 2.6, and 3.3 layers at a temperature of $\lesssim 11$ K are shown in Fig. 3. Remarkably, we find no change in the patterns between $\Theta=1.67$ and 2.60. This can be seen by comparing the fit of the solid curve from Fig. 2(b), calculated for the pinwheel model of the TI phase, to both patterns. We emphasize that the solid curve has not been rescaled at $\Theta=2.60$. On the other hand, we do observe a change in the diffraction pattern from $\Theta=2.60$ to 3.30. The main peak near $Q=1.8$ Å^{-1} increases in both height and width. In another scan at $\Theta=3.30$ (not shown), we did not reproduce the increase in peak height at $Q=1.8$ Å^{-1}, but did observe the same increase in width.[14] Also, as shown in Fig. 3(b), for $\Theta=3.30$ there is an increase in the scattering at higher Q with the peak at $Q=4.1$ Å^{-1} becoming more prominent.

We interpret the coverage dependence of the diffraction patterns in Fig. 3 as follows. Recall that a

coverage $\Theta=1.67$ is required to fully compress the monolayer at which point it is in the TI phase. As noted in Sec. III A, about 30% of the molecules occupy the *second* layer at this coverage.[15] In Ref. 1 we suggested that these second-layer molecules were either amorphous or in a highly disordered state, and hence any peaks which they might contribute to the diffraction pattern would be broad and too weak to be observed. We now use the same argument to explain the similarity in the patterns at $\Theta=1.67$ and 2.60. In this coverage range the observed diffraction patterns do not change because there is a continued filling of amorphous second and third layers. At higher coverages $\theta=2.60$ and 3.30 the increase in height and width of the main peak at $Q=1.8$ Å^{-1} [see Fig. 3(a)] can be understood if there is crystallization of a bilayer, as we discuss below.

In this interpretation the occupancy of the second and third layers at a coverage $\Theta=2.60$ is not easily inferred. If the amorphous second layer contains about the same number of molecules as the first layer (as is the case for the bilayer crystal—see Sec. III C), then the third layer would have only $\frac{1}{3}$ as many. However, if the second layer is highly disordered it may have a lower density than in the bilayer crystal, resulting in a higher third-layer occupancy. At a coverage $\Theta=3.30$, where the bilayer has crystallized, the number of molecules in the first two layers corresponds to a coverage $\Theta=2.21$. The third layer would be nearly complete, if it had the same density as the first two. However, if it is amorphous, there could be occupancy of fourth and higher layers.

As shown in Fig. 4, at coverages above $\Theta=3.3$ and temperatures ~ 11 K, new peaks (labeled $i-q$) appear in the diffraction patterns. These peaks can be indexed according to the cubic structure of bulk α-N_2 (Ref. 16) and grow in intensity as the coverage increases. The integrated intensity of the (200) peak (labeled i) is determined most easily because it does not overlap with other bulk peaks, and the contribution of the main film peak at $Q=1.8$ Å^{-1} can be separated by a line-shape analysis. The plot of the (200) integrated peak intensity in Fig. 5 shows it to decrease linearly with coverage extrapolating to zero at $\Theta\simeq 3.7$, where bulk nucleation presumably occurs.

To summarize our interpretation of these results, we infer that two amorphous or highly disordered N_2 layers form initially above the fully compressed TI monolayer phase. At a loading of $\Theta\simeq 3.0$ the ordered first layer and the disordered second layer crystallize into a bilayer structure, leaving an amorphous third layer. As the coverage is increased further, molecules continue to enter the disordered film above the bilayer crystal until bulk nucleation occurs at $\Theta\simeq 3.7$.

C. Structure of the crystal bilayer

As discussed in Sec. III B, we attribute the change in the diffraction patterns between $\Theta=2.60$ and 3.30 in Fig. 3 to the crystallization of the bilayer. This interpretation is supported by bilayer profile calculations which reproduce the increase observed in both the height and width of the main peak at $Q=1.8$ Å^{-1} between these two coverages. The bilayer crystal should contribute to the diffraction patterns at all coverages $\Theta\gtrsim 3.30$ (see Fig. 4). Unfortunately, the bulk Bragg peaks overlap with those of the bilayer and are too intense to allow a bilayer structural analysis. Therefore, in this section we only attempt to fit the $\Theta=3.30$ pattern to different bilayer crystal models. As before, we assume that scattering from disordered layers above the bilayer crystal do not contribute significantly to the diffraction pattern.

We first investigated a bilayer model in which both layers were constrained to have the herringbone structure of Fig. 1(a). The relative position of the two layers with respect to a plane parallel to the surface is illustrated in

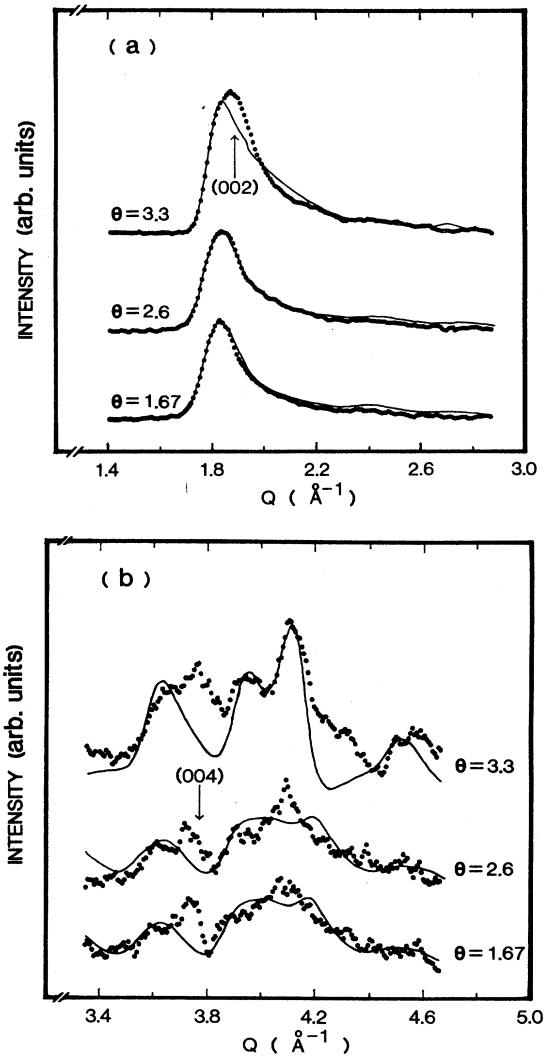

FIG. 3. Coverage dependence of the diffraction patterns below 11 K at coverages near crystallization of the bilayer: (a) low-Q region and (b) high-Q region. At each coverage, the diffracted neutron intensity has been scaled to the same number of monitor counts in the incident beam. The *same* solid curve from Fig. 2(b) has been superimposed on the patterns at $\Theta=1.67$ and 2.60. The solid curve at $\Theta=3.3$ is calculated for the pinwheel model of the bilayer in Fig. 7(b).

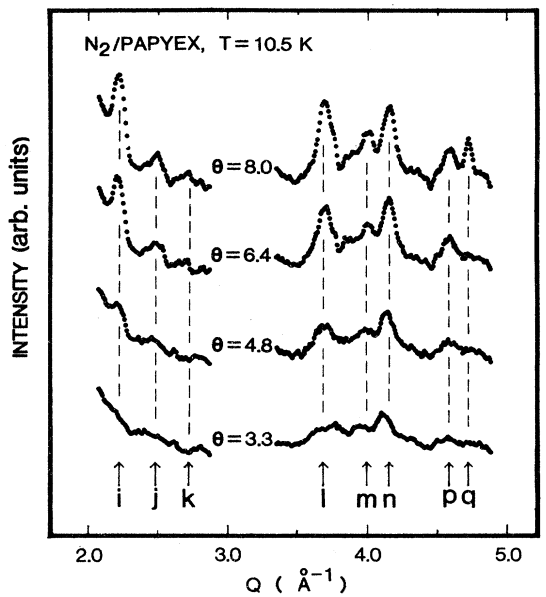

FIG. 4. Coverage dependence of the diffraction patterns at 10.5 K above $\Theta=3.30$ layers. At each coverage the diffracted neutron intensity has been scaled to the same number of monitor counts in the incident beam. The letters correspond to the positions of the bulk α-N_2 peaks as follows: $i=(200)$, $j=(102)$, $k=(112)$, $l=(113)$, $m=(203)$, $n=(213)$, $p=(104)$, and $q=(114)$.

Fig. 6(a). As a starting point for the fitting procedure, we chose the ϕ and β values obtained for the herringbone model of the monolayer TI phase, at $\Theta=1.67$ (see Table I). The best fit which could be obtained to the $\Theta=3.30$ diffraction pattern is shown by the solid curve in Fig. 7(a) corresponding to the structural parameters listed in Table II. The unit cell is slightly oblique [$\gamma=89.2°$ in Fig. 6(a)]

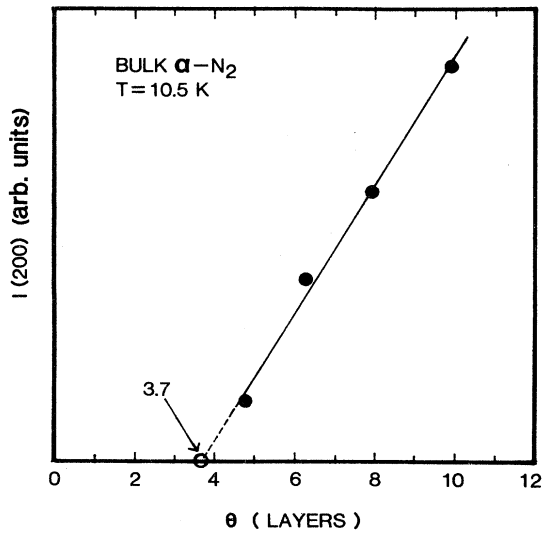

FIG. 5. Integrated intensity of the (200) peak of bulk α-N_2 versus coverage. Error bars are less than the size of the data points.

with the magnitude of both lattice vectors compressed about 5% from those of the C monolayer phase. We see that the molecules' azimuthal orientation $|\phi|$ changes from 135° in the TI phase to 125° for the herringbone bilayer. Also, the tilt angle β increases by 5° in the first layer and 10° in the second layer over its value in the TI phase. The second-layer molecule centers of mass are situated 2.85 Å above the center of a triangle of three first-layer molecules. The Debye-Waller factor was kept at the same value as for the TI phase, $\langle u^2\rangle=0.03$ Å^2.

Unfortunately, the line-shape analysis of the main bilayer or {20} peak at $Q=1.8$ Å^{-1} is affected by the close proximity of the graphite (002) reflection. We have identified the {20} bilayer peak position with the small shoulder near the top of the leading edge of the large peak observed. The observed peak maximum actually

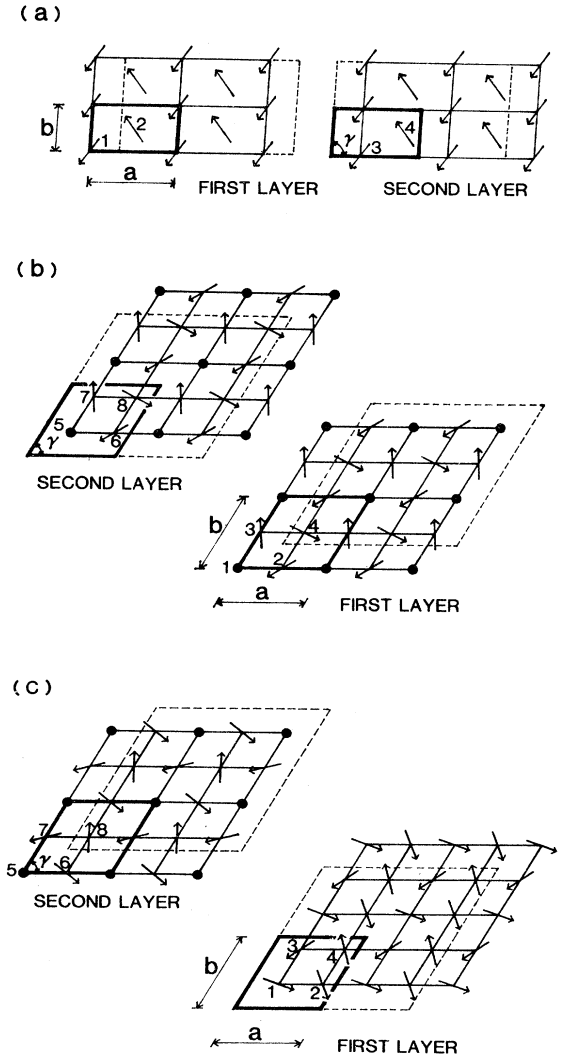

FIG. 6. Schematic diagrams of three bilayer crystal models: (a) herringbone bilayer, (b) pinwheel bilayer, and (c) herringbone first layer–pinwheel second layer. The azimuthal orientation ϕ and tilt angle β of the molecules are measured as in Fig. 1.

occurs at $Q=1.89$ Å^{-1}, the wave-vector transfer of the graphite (002) reflection. We explain this by imperfect subtraction of the scattering from the graphite substrate or possibly a coherent interference effect[17] between the bilayer and graphite scattering for **Q** directed along the surface normal. Attempts to identify the bilayer {20} peak with the maximum in the observed peak resulted in poorer fits to the diffraction pattern at higher Q. Despite this difficulty in analyzing the {20} line shape, we conclude that the calculated profile for the herringbone bilayer structure gives too much intensity in its trailing edge near $Q=2.2$ Å^{-1}. The model also fails to give enough intensity near a small peak observed at $Q=4.5$ Å^{-1}. The only other discrepancies between the calculated profile and the observed pattern occur near the graphite (004) and aluminum (220) reflections, where imperfect background subtraction is suspected.

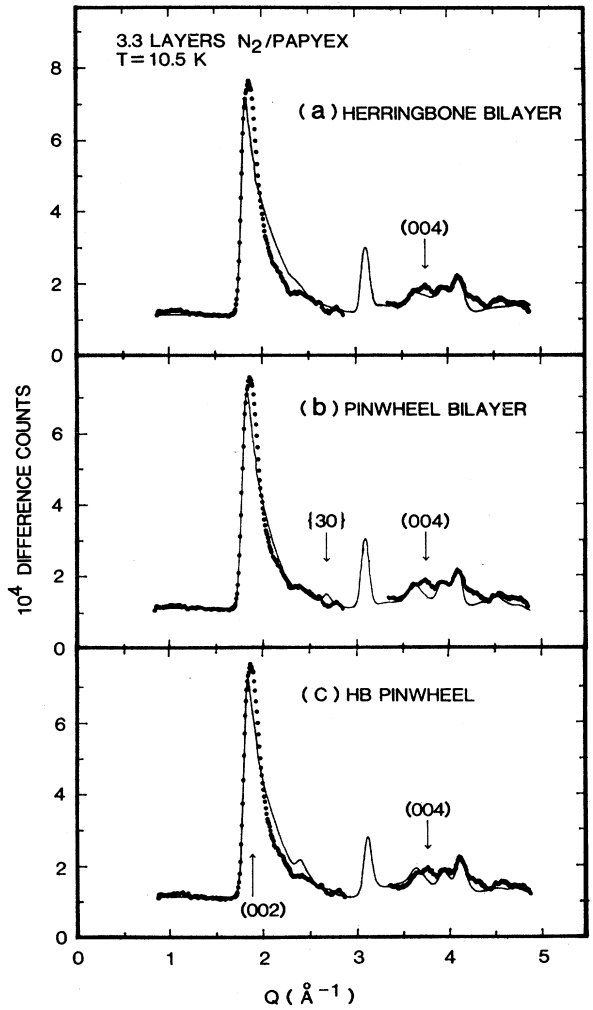

FIG. 7. Diffraction pattern of 3.30 layers of N_2 on Papyex at 10.5 K after the substrate scattering has been subtracted (same data as in Figs. 3 and 4). The solid curves have been calculated using the parameters listed in Table II for (a) the bilayer herringbone model, (b) the bilayer pinwheel model, and (c) the herringbone-pinwheel model depicted in Fig. 6. A different constant value has been added to the calculated curves above the graphite (002) reflection ($Q=1.88$ Å^{-1}) than below.

We have also fitted a profile corresponding to a bilayer pinwheel model to the $\Theta=3.30$ diffraction pattern. In this case we assumed each layer to have a pinwheel structure so that the bilayer unit cell contained eight molecules as shown schematically in Fig. 6(b). To fit the Bragg peak positions, a nonhexagonal unit cell ($a\neq b$) was required. For initial values of the orientational parameters ϕ and β, we chose a set determined by Bruch[13] in ground-state calculations. The solid curve in Fig. 7(b) shows the best fit obtained corresponding to the structural parameters listed in Table II. The fit yields a bilayer density which is nearly the same as for the herringbone model. In the fit, molecules no. 1 and no. 5 were constrained to be perpendicular to the surface while the height z of each molecule was fixed at its calculated[13] value. The angles β and ϕ of the three nonperpendicular molecules in the first layer are found to be about the same as for the pinwheel model of the fully compressed (TI) monolayer phase. However, the second-layer molecules have a tilt β about 15° larger than in the TI phase pinwheel model. (As before, the β angles for the nonperpendicular molecules in each layer are constrained to be equal). The second-layer molecules are again centered over a triangle of three first-layer molecules, but their center of mass is almost 0.5 Å higher than for the herringbone model.

The calculated profile for the pinwheel bilayer model fits the trailing edge of the main peak better than for the herringbone bilayer structure. It also gives a better fit to the weak peak at $Q=4.5$ Å^{-1} for the same Debye-Waller factor $\langle u^2\rangle=0.03$ Å^2. However, the small {30} peak predicted at $Q=2.7$ Å^{-1} is not observed.

Our last attempt to fit the bilayer diffraction pattern was based on the model of Kuchta and Etters.[7] As discussed in Sec. I and illustrated in Fig. 6(c), their Monte Carlo calculations predicted a "disordered" herringbone structure for the first layer and a pinwheel structure for the second layer. Notice that there are four molecules in the first layer of the unit cell in Fig. 6(c) compared to two in Fig. 6(a) so that there are still a total of eight molecules per unit cell as in the pinwheel bilayer model. The solid curve in Fig. 7(c) is the best fit to the diffraction pattern obtained for the parameters listed in Table II. Each of the structural parameters was allowed to relax from its calculated value[7] except for the heights of the second-layer molecules. The experimentally inferred structure has the density calculated by Kuchta and Etters, but not the hexagonal symmetry which they assumed. The lattice vectors found are the same as for our fit to the bilayer pinwheel model. The center of mass of each nonperpendicular second-layer molecule is at a height of 3.03 Å above the first layer—a value intermediate between those of the herringbone and pinwheel bilayer models. As for the orientational parameters, all of the values listed in Table II are within ±5° of those calculated by Kuchta and Etters.[7]

In the trailing edge of the main diffraction peak, the quality of fit for the Kuchta-Etters model is about the

TABLE II. Structural parameters for the N_2 bilayer crystal on graphite inferred from the diffraction pattern at a coverage $\Theta = 3.30$ layers and a temperature of 10.5 K (Fig. 7). Three different bilayer models are considered: herringbone, pinwheel, and herringbone (first layer)–pinwheel (second layer). The labels I and II refer to the first and second layers, respectively. All parameters are defined as in Table I. Subscripts denote molecule number defined in Fig. 6. The center-of-mass heights z of the second-layer molecules are measured with respect to the plane containing the first-layer centers of mass (in the case of the pinwheel first layer, this plane is defined by the centers of mass of the three nonperpendicular molecules).

	Herringbone		Pinwheel		Herringbone–pinwheel	
	I	II	I	II	I	II
a (Å)	7.01	7.01	8.04	8.04	8.04	8.04
b (Å)	4.05	4.05	8.16	8.16	8.16	8.16
γ	89.2	89.2	60.0	60.0	60.0	60.0
ρ	1.107	1.107	1.107	1.107	1.107	1.107
ϕ_1,ϕ_5	−125	−125			−20	
ϕ_2,ϕ_6	125	125	−147	−147	−70	−40
ϕ_3,ϕ_7			93	93	−145	−165
ϕ_4,ϕ_8			−27	−27	105	88
β_1,β_5	25	30	90	90	10	90
β_2,β_6	25	30	8	24	10	15
β_3,β_7			8	24	10	15
β_4,β_8			8	24	10	15
z_1,z_5 (Å)	0	2.85	0.294	3.29	0	3.23[a]
z_2,z_6 (Å)	0	2.85	0	3.32	0	3.03[a]
z_3,z_7 (Å)			0	3.32	0	3.03[a]
z_4,z_8 (Å)			0	3.32	0	3.03[a]
L (Å)	95	95	95	95	95	95
$\langle u^2 \rangle$ (Å^2)	0.03	0.03	0.03	0.03	0.03	0.03

[a]R. D. Etters (private communication).

same as that obtained for the pure herringbone bilayer structure. The fit is not quite as good as for the other models at $Q > 3.2$ Å^{-1}.

To summarize, we have found that the diffraction pattern attributed to the crystal bilayer can be fitted reasonably well by several physically plausible models. For all of these models, the two N_2 layers are commensurate with each other and have a density slightly less than in either the herringbone or pinwheel model of the fully compressed monolayer (TI) phase (see Table I). Due to the lower binding energy of the second layer to the substrate, one might expect a slightly lower packing density than in the first layer.[18] The first-layer expansion of 0.5–1.1 % in area from that of the TI phase may be necessary in order that the two N_2 layers remain commensurate.

D. Search for a layering transition

In an effort to confirm the existence of the layering transition at 23.4 K inferred by Zhang *et al.*[8] from their heat-capacity data, we have obtained diffraction patterns as a function of temperature at coverages $\Theta = 6.4$ and 8.0 layers. Our intent was to look for an intensity decrease in the Bragg peaks of the coexisting bulk phase as a signature of layering. This method has been successful in investigating the layering transitions of ethylene[19] and iron pentacarbonyl[20] on graphite by x-ray scattering.

In Fig. 8 we show the neutron-diffraction patterns from a 6.4-layer sample at 10.5 and 26.0 K. These temperatures are, respectively, below and just above 23.4 K, the temperature at which a large heat-capacity peak is observed.[8] We see that all of the bulk peak intensities with the possible exception of the ones labeled l and n in Fig. 8(b) are temperature independent. This is shown with greater sensitivity for the bulk (200) peak in the inset of Fig. 8(a). If the amount of bulk material had decreased as a result of a layering transition, we would expect the integrated intensity of each of the bulk peaks to decrease by about $\frac{1}{3}$.[21] Thus our data do not support a transition from two-layer–plus–bulk to three-layer–plus–bulk as the sample is heated through 23.4 K.

In an effort to find an explanation of the heat-capacity peak at 23.4 K which is consistent with our neutron-diffraction results, we have considered the possibility of it being caused by the melting of the second layer of the bilayer crystal. If such were the case, it is likely that the ~ 1.5 layers of disordered material above the bilayer crystal would also become mobile. Thus above 23.4 K there would be a solid first layer covered by a total of ~ 2.5 fluid layers. Like the upper amorphous layers, this fluid component should produce broad and weak peaks which are difficult to resolve in the presence of the Bragg peaks of the coexisting bulk phase (for the 6.4-layer sample, the bulk material corresponds to a coverage of about 2.8 layers). For this reason, we have also obtained diffraction patterns from a 3.30-layer sample at 28.6 and 32 K (not shown) which do not contain a bulk component. A small increase in the scattering at low Q (< 1.8 Å^{-1}) charac-

teristic of a fluid film[20] is observed. However, this low-Q scattering is too weak to analyze quantitatively.

IV. DISCUSSION AND CONCLUSIONS

We have found both herringbone and pinwheel models to be consistent with the neutron-diffraction pattern of the fully compressed monolayer or TI phase. This result conflicts with the conclusion of LEED experiments[22] which found a pinwheel model to be incompatible with the TI-phase diffraction pattern. Recent ground-state calculations[13] indicate a pinwheel structure to become energetically favorable as the monolayer is compressed beyond the UI phase. As a result of our analysis here, we now have an explicit set of experimentally inferred structural parameters (see Table I) for comparison with these calculations.

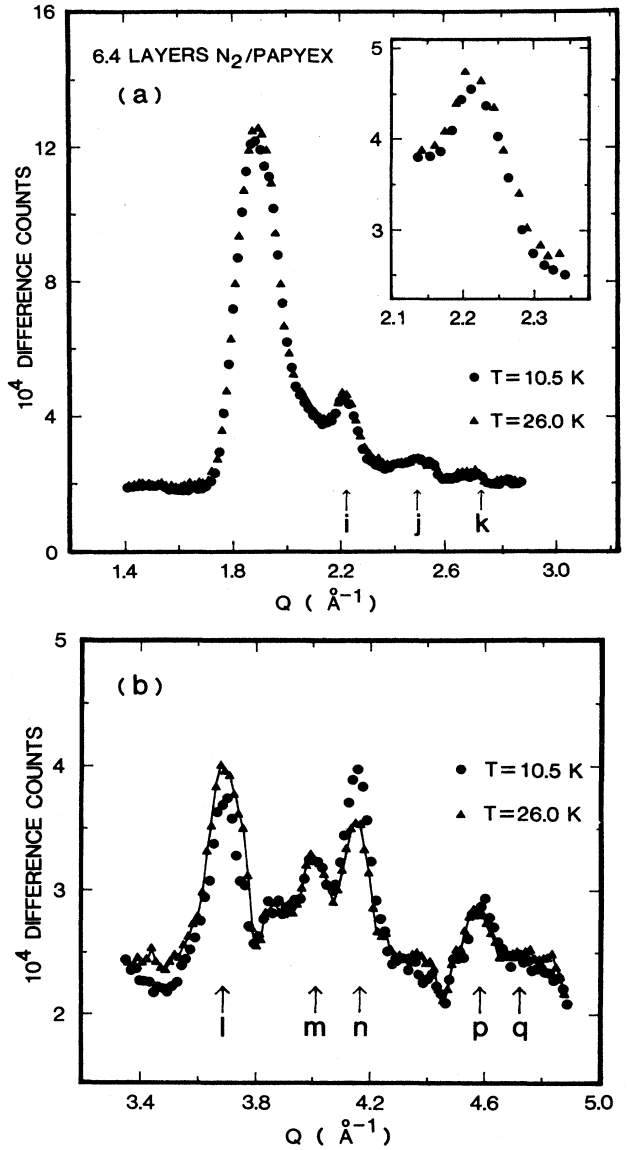

FIG. 8. Diffraction pattern of the 6.4-layer film at temperatures of 10.5 and 26.0 K: (a) low-Q region and (b) high-Q region. Inset in (a) shows with greater sensitivity the temperature independence of the peak labeled i corresponding to the bulk (200) peak of α-N_2. The labeling of the other peaks is the same as in Fig. 4. The solid curve in (b) is a guide to the eye through the high-temperature points.

Obviously, further ground-state calculations investigating a pinwheel structure for the TI phase would be desirable. These calculations should allow for a small distortion of the lattice from hexagonal symmetry. It would also be helpful if they addressed other experimentally observed features of the TI phase. One of these is the large coexistence region between the UI and TI phases at low temperature.[1] Another is the absence of a specific-heat anomaly associated with an orientational-disordering transition in the coexistence region.[8,23] Both of these features suggest that there could be more orientational disorder present in the nominally pure TI phase than in the submonolayer C phase. This is supported by the lower coherence length in the TI phase of 60 Å (see Table I) compared to 105 Å in the C phase (from Ref. 1) and 95 Å in the bilayer crystal (see Table II). In order to investigate the degree of orientational disorder, it would be useful to supplement further ground-state calculations with Monte Carlo and molecular-dynamics simulations using the same potentials.

Our analysis of the $\Theta=3.30$ diffraction pattern in Fig. 7 does not allow a definitive determination of the orientational order in the bilayer crystal. Nevertheless, there are several structural features which are common to all three models which we have investigated. First, the layer density of the bilayer crystal is slightly less than that of the fully compressed monolayer phase. Second, the two N_2 layers are of equal density and commensurate. And third, the layers are slightly distorted from hexagonal symmetry.

In Table II we have listed explicit parameter sets for the three different models of the crystal bilayer. As for the TI phase, further ground-state calculations which allow for a distortion of the layers from hexagonal symmetry would be valuable for comparison. Although not conclusive, we would like to present some arguments favoring a pinwheel structure for each layer or possibly a structure with some orientational disorder in the first layer and a pinwheel structure in the second layer. A potential problem with the bilayer herringbone model is that, in order to obtain a satisfactory fit, the second-layer height had to be lowered to $z=2.85$ Å or 5% less than that calculated by either Bruch[13] or Kuchta and Etters[7] and 14% less than used by Vernov and Steele.[6] On the other hand, we note that the only deficiency of the pinwheel bilayer model in Fig. 7(b) is the weak {30} peak predicted but not observed. This peak weakens when the first layer assumes a distorted herringbone structure as in the Kuchta-Etters model. A scenario which would be consistent with all of our data is that the fully compressed monolayer has a pinwheel structure but expansion of the first layer to crystallize the bilayer introduces appreciable orientational disorder into it. This orientational disorder may not be exactly of the type which Kuchta and Etters have calculated—the structure may be more pinwheel-like as in the (111) plane of bulk

α-N_2.

Perhaps more important than the actual bilayer crystal structure in understanding the incomplete wetting of the film is the apparent role which disorder plays in its growth process. In Ref. 1, we showed that about half of a disordered second layer is required to fully compress the monolayer. Here we have seen that the bilayer does not crystallize until about two layers of disordered material have accumulated above the fully compressed monolayer. Also, after bilayer crystallization, about 1.5 layers of disordered material adsorbs prior to bulk nucleation. The presence of disordered material both before and after bilayer crystallization suggests that there could be an appreciable amount of orientational disorder within the bicrystal as well. Thus it is tempting to attribute the incomplete wetting to structural disorder appearing in the early stages of the solid film growth. However, another factor which might inhibit trilayer formation is the lower layer density $\rho=1.11$, which we find for the bilayer (see Table II) compared to the value $\rho=1.14$ which Kuchta and Etters[7] calculate for the (111) plane of bulk α-N_2. Also, the distortion of the bilayer from hexagonal symmetry may affect the trilayer stability adversely. Monte Carlo and molecular-dynamics simulations could be very helpful in addressing the question of whether structural disorder in the bilayer contributes to the incomplete wetting of the N_2 film.

The temperature independence of the Bragg peak intensities of the bulk phase coexisting with the film has provided strong evidence against a layering transition as proposed in Ref. 8. We have suggested instead that the large heat-capacity peak observed at 23.4 K for coverages $\Theta \gtrsim 3$ results from the melting of the top layer of the bicrystal. The much greater size of this heat-capacity anomaly compared to those associated with orientational disordering of the molecules supports the view that some translational disorder is introduced into the film. Because the second layer resides on the relatively corrugated surface of the orientationally ordered first layer, the proposed second-layer fluid may be more correlated just above the melting point (with respect to both molecular orientations and translations) than the submonolayer fluid at the corresponding temperature. A small increase in the low-Q scattering of a 3.30-layer sample was observed above 23.4 K. While this behavior is characteristic of a well-correlated fluid component, further measurements are required to substantiate this interpretation. We cannot, therefore, exclude the possibility of another type of phase transition occurring.

A second-layer melting point of 23.4 K may seem low compared to the melting point of the *completed C* monolayer phase which exceeds the bulk triple point $T_t=63$ K. However, the submonolayer C phase melts at 50 K,[24] which is closer to the range (50–70 % of T_t) typical of monolayers physisorbed on graphite. From this perspective, a melting point at 23.4 K (37% of T_t) appears plausible for the second layer. Clearly a molecular-dynamics study could be helpful in estimating the N_2 bilayer melting point. No evidence of second-layer melting was seen in previous molecular-dynamics simulations of the bilayer at 25 and 35 K.[6]

The second-layer melting hypothesis implies a phase diagram differing greatly from that proposed in Ref. 8. In the remaining discussion, we describe a new phase diagram shown in Fig. 9 which we have attempted to construct to be consistent with both the heat-capacity and neutron-diffraction data. The points in the phase diagram correspond to the location of heat-capacity peaks observed by Zhang *et al.*[8] The second-layer melting line (solid squares) can be seen at $\sim$23.4 K. It has been extended as a dashed line below $\theta\sim2.7$ to suggest that there might be some mobility change near this temperature in the disordered or amorphous (A) material above the fully compressed monolayer solid labeled 1SO. (The O denotes orientationally ordered; similarly, 2SO denotes the orientationally ordered bilayer crystal.)

As in Ref. 8, we associate the vertical lines near 29 K (circles) with orientational-disordering transitions. However, since we are now interpreting the second layer as being fluid (F) at this temperature, this transition must occur in the first-layer solid. We have been unable to identify a structural change in the 1S phase which correlates with the depression in the transition temperature near $\Theta=2.4$. We speculate that an expansion of 1S to a

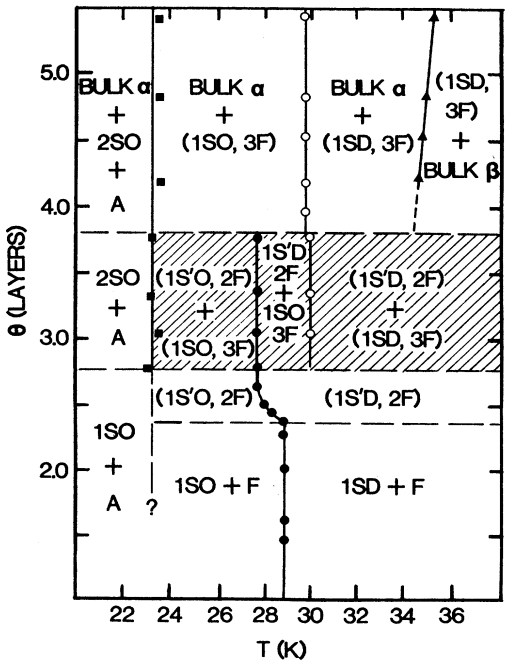

FIG. 9. Proposed phase diagram of multilayer N_2 on graphite. 1S, 1S′, and 2S denote the fully compressed monolayer solid (TI) phase, expanded monolayer phase, and bilayer crystal phases, respectively. A denotes an amorphous phase as described in the text and nF the fluid phase where n is the number of fluid layers. The symbols indicate positions of heat-capacity peaks from Fig. 2 of Ref. 8. The solid squares correspond to the second-layer melting transition, the solid and open circles to the orientational-disordering transition in the 1S′ and 1S phases, respectively, and the solid triangles to the bulk α-β transition. Hatched region denotes coexistence of the 1S and 1S′ phases. O and D denote orientationally ordered and disordered phases, respectively.

phase 1S′ might occur which anticipates that required for bilayer crystallization. Expansion of the monolayer lattice would presumably lower the barrier to rotational motion, thereby reducing the transition temperature for orientational disordering. We note, though, that below 11 K no expansion can be resolved between $\Theta=1.6$ and 2.6 in the diffraction patterns of Fig. 3.

We speculate that the 1S phase is reentrant at higher coverages due to compression from the thickening fluid layers adsorbed above the solid monolayer. This provides an explanation for the increase in the orientational-disordering transition temperature from ~ 28 K in the 1S′ phase to ~ 30 K for $\Theta \gtrsim 2.8$.[25] For $2.8 \lesssim \Theta \lesssim 3.8$ we postulate coexistence between the 1S and 1S′ phases (hatched region in Fig. 9). In this coexistence region the fluid film thickness would vary from two (2F) to three (3F) layers across a surface with the reentrant 1S phase being present under the thicker fluid regions. At coverages $\Theta \gtrsim 3.7$, bulk N_2 nucleates and the 1S′ phase disappears near completion of the third fluid layer ($T > 23.4$ K). We emphasize the tentative nature of this phase diagram and recognize that there may be other ways to reconcile the neutron and heat-capacity data.

ACKNOWLEDGMENTS

The authors would like to thank L. W. Bruch, M. H. W. Chan, R. D. Etters, S. C. Fain, Jr., F. Y. Hansen, J. Z. Larese, S. F. O'Shea, L. Passell, W. A. Steele, and D. J. Tildesley for discussion of our results. We are especially indebted to L. W. Bruch for communicating results of his calculations prior to publication and for comments on this manuscript. This work was supported by National Science Foundation Grant Nos. DMR-8304366 and DMR-8704938 and U.S.-Israel Binational Science Foundation Grant Nos. 2687 and 86-00294.

*Present address: Bell Laboratories, 1255 S. Cedar Crest Blvd., Allentown, PA 18103.

†Present address: Physics Department, Utah State University, Logan, UT 84322.

[1]R. Wang, S.-K. Wang, H. Taub, J. C. Newton, and H. Shechter, Phys. Rev. B **35**, 5841 (1987).

[2]J. L. Seguin, J. Suzanne, M. Bienfait, J. G. Dash, and J. A. Venables, Phys. Rev. Lett. **51**, 122 (1983).

[3]R. D. Diehl and S. C. Fain, Jr., Surf. Sci. **125**, 116 (1983).

[4]A. B. Harris and A. J. Berlinsky, Can. J. Phys. **57**, 1852 (1979).

[5]S. F. O'Shea and M. L. Klein, Phys. Rev. B **25**, 5882 (1982).

[6]A. Vernov and W. A. Steele, Surf. Sci. **171**, 83 (1986).

[7]B. Kuchta and R. D. Etters, Phys. Rev. B **36**, 3400 (1987).

[8]Q. M. Zhang, H. K. Kim, and M. H. W. Chan, Phys. Rev. B **33**, 413 (1986).

[9]Manufactured by Le Carbone Lorraine, Département Produits Speciaux, 37 à 41 rue Jean Jaurès, 92231 Gennevilliers, France.

[10]J. K. Kjems, L. Passell, H. Taub, J. G. Dash, and A. D. Novaco, Phys. Rev. B **13**, 1446 (1976).

[11]G. J. Trott, H. Taub, F. Y. Hansen, and H. R. Danner, Chem. Phys. Lett. **78**, 504 (1981).

[12]G. J. Trott, Ph.D. thesis, University of Missouri–Columbia, 1981.

[13]L. W. Bruch (private communication). "Ground-state" calculations refer to static potential-energy calculations performed by Bruch.

[14]The irreproducibility of the peak height may have been due to electronic instability of the position-sensitive detector (see Ref. 1) which caused imperfect subtraction of the graphite (002) peak.

[15]This conclusion holds for both the "two-out" herringbone and pinwheel models discussed in Sec. III A.

[16]A. F. Schuck and R. L. Mills, J. Chem. Phys. **52**, 6000 (1970).

[17]H. Taub, K. Carneiro, J. K. Kjems, L. Passell, and J. P. McTague, Phys. Rev. B **16**, 4551 (1977).

[18]J. Z. Larese, M. Harada, L. Passell, J. Krim, and S. Satija, Phys. Rev. B **37**, 4735 (1988).

[19]M. Sutton, S. G. J. Mochrie, R. J. Birgeneau, D. E. Moncton, and P. M. Horn, Phys. Rev. B **30**, 263 (1984).

[20]J. R. Dennison, H. Taub, F. Y. Hansen, H. Shechter, and R. Brener, Phys. Rev. B **37**, 2266 (1988).

[21]Assuming bulk nucleation at coverage $\Theta=3.7$ layers from Fig. 5, the bulk particles will constitute 2.7 layers of material for a total coverage $\Theta=6.4$. If a layering transition were to occur, the amount of bulk material would decrease from 2.7 to 1.7 layers, i.e., by 37%.

[22]H. You and S. C. Fain, Jr., Faraday Discuss. Chem. Soc. **81**, 159 (1985).

[23]Q. M. Zhang, H. K. Kim, and M. W. H. Chan, Phys. Rev. B **32**, 1820 (1985).

[24]A. D. Migone, M. W. H. Chan, K. J. Niskanen, and R. B. Griffiths, J. Phys. C **16**, L1115 (1983).

[25]The higher transition temperature of 30 K for orientational disordering in the reentrant 1S phase compared to 29 K in the 1S phase at lower coverages could result from a flattening effect of the upper fluid layers (see Ref. 6). If the N—N bond of the molecules in the first layer is more nearly parallel to the surface, the barrier to rotation about the surface normal would increase. Alternatively, one might postulate a slightly higher density for the reentrant 1S phase than at lower coverages.